Extracting Nucleation Rates from Ramped Temperature Measurements of Gas Hydrate Formation

Mark T.J. Barwood[1], Peter J. Metaxas[1], Vincent W.S. Lim[1], Catherine C. Sampson[1], Michael L. Johns[1], Zachary M. Aman[1], and Eric F. May[1]*

1. Fluid Science & Resources, School of Engineering, University of Western Australia, 35 Stirling Highway, Perth, WA 6009, Australia

*Corresponding author: eric.may@uwa.edu.au

Abstract

The formation of solids in the energy industry poses a threat to safety and reliability of operational facilities across numerous process stages. Experimental studies of gas hydrate formation probability are conducted under both fixed-temperature and ramped-temperature conditions. Although a method to extract nucleation rates from constant temperature measurements of induction time probability distributions is well established, extracting such rates from constant cooling data is complicated by the time-dependent driving force for hydrate formation. Here, we present and use a method for extracting the stationary nucleation rate as a function of temperature from constant cooling experiments based on the hazard function, which accounts for the system's history and the instantaneous formation probability. This method yields nucleation rates consistent with those measured using more time-consuming constant temperature experiments, while providing far more information about the underlying nucleation phenomena by sampling a wider range of temperatures. Measurements of methane hydrate formation probability obtained in well-mixed systems at 12 MPa with temperature ramp rates (1 – 3) $K \cdot min^{-1}$ were analysed using a framework based on Classical Nucleation Theory. The results suggest that the heterogeneous nucleation sites primarily responsible for

the observed nucleation rate become more numerous and have higher average energy barriers as subcooling increases. This hypothesis is also consistent with recent experimental studies of systems containing kinetic hydrate inhibitors and provides a pathway to more reliable predictions of hydrate formation probability in production systems that experience a wide range of subcoolings.

Introduction

During the production of natural gas from oil and gas reservoirs, gas hydrates (ice-like inclusion compounds) can form at the high pressure and low temperatures that are present in subsea pipelines, posing a blockage risk [1-3]. These compounds are also stable in permafrost and on the floor of deep oceans [4], and find application areas including water desalination [5] as well as gas separation and storage (including carbon capture) [6]. Alongside hydrate growth rates [7], quantifying the likelihood of hydrate formation is essential to characterising the risk of these dangerous and costly blockages in industrial natural gas production systems [3]. However, this characterisation is challenging due to the stochastic nature of hydrate nucleation, meaning both the formation temperature and induction ("wait") time associated with such events are randomly distributed variables (both with and without the presence of chemical oilfield additives) [8-15].

Central to quantifying hydrate formation risk is a determination of the nucleation rate, J, the inverse of which corresponds to the mean time required to form a supercritical nucleus able to grow into a macroscopic solid. The nucleation rate is a function of the thermodynamic driving force for solid formation, typically quantified *via* the supersaturation, $\Delta\mu$ [16, 17] of the system. A common and convenient experimental measure of the driving force for hydrate nucleation is the system's subcooling, ΔT, which is proportional to $\Delta\mu$ under isobaric conditions [2, 16, 17].

$$\Delta T = T_{eq} - T \tag{1}$$

Here, T_{eq} is the hydrate equilibrium temperature at the formation pressure, and T the formation temperature. According to Classical Nucleation Theory (CNT) [17], the dependence of J on ΔT is given by:

$$J = A \exp\left(\frac{\Delta s_e \Delta T}{k_B T}\right) \exp\left(-\frac{B'}{T\Delta T^2}\right) \tag{2}$$

Here, A is the kinetic nucleation parameter, Δs_e the entropy of solid dissociation ($22.2 k_B$ for methane hydrate), k_B the Boltzmann constant, and B' the thermodynamic nucleation parameter.

In isothermal experiments at constant ΔT, the mononuclear mechanism considered by CNT leads to an exponential distribution of induction times with a constant J [16].

$$F(t) = 1 - \exp(-Jt) \tag{3}$$

Here $F(t)$ is the cumulative formation probability at time, t. The ability of Eq (3) to describe induction time probability distributions has been verified extensively for gas hydrates formed in a variety of systems with different sizes and boundary conditions, including autoclaves [18], small stirred reactors [15, 19, 20], and acoustically levitated droplets [21, 22].

An alternative method of extracting stationary nucleation rates at constant subcooling is *via* the hazard function, $h(t)$, which is commonly used in survival analysis [23]. This function quantifies the likelihood of an event occurring between times t and $t + dt$ given it has not occurred prior to time t [24, 25].

$$h(t) = \frac{f(t)}{1 - F(t)} \tag{4}$$

Here, $f(t)$ is the formation probability density function (the derivative of the cumulative formation probability function $F(t)$). For an exponential cumulative probability distribution with constant rate parameter J, $h(t)$ becomes equivalent to the nucleation rate

$$h(t; \text{constant } J) = \frac{J \exp(-Jt)}{1 - (1 - \exp(-Jt))} = J \quad (5)$$

If a discrete approximation for $f(t)$ is obtained from repeated measurements at constant subcooling (e.g. a histogram of formation events is constructed as in refs. [10-12, 21, 22, 26]), a value of J may be estimated by one of two methods, both of which require (numerical) integration of the probability density distribution to give the cumulative probability distribution. Either the measured $F(t)$ can be fit to Eq (3), or the hazard function $h(t)$ can be constructed and J estimated at each finite value of t. Constructing $h(t)$ additionally affords a quantitative test of whether the nucleation rate is actually stationary (for which $h(t)$ should be constant). A time-dependent nucleation rate may not be evident if only the quality of the data's fit to Eq (3) is considered, especially considering induction times can vary over many orders of magnitude. However, if the nucleation rate is truly stationary as expected at constant temperature, these two methods should give the same result.

A limitation of constant temperature measurements is the limited sample of J values which can be explored due to the small range of experimentally accessible subcoolings. At low subcoolings, induction time experiments become impractically long, while at high subcoolings, formation can occur while the apparatus is still being cooled, and thus prior to reaching the target formation temperature [15]. An alternative method of measuring formation probability at higher subcoolings is to ramp the system temperature (at a constant rate) into the solid stability region and record the formation temperature (as in refs [10-12, 26-29]). Furthermore, by varying the ramp rate, numerous independent formation events over a wide range of temperature can be measured more rapidly than *via* the acquisition of induction time distributions at fixed ΔT [12]. The cooling rate selected for the ramp does not affect the measurement of the dependence of J on subcooling, as is demonstrated here experimentally.

Extracting accurate nucleation rates from ramped experiments can, however, be non-trivial [30] with previous results demonstrating clear rate dependencies for J [28, 29, 31, 32]. May et al. [11] proposed fitting Eq (6) to subcooling distributions measured for methane hydrates using a high-pressure stirred automated lag time apparatus (HPS-ALTA) along multiple (> 100) cooling ramps.

$$F(\Delta T) = 1 - \exp\left(-A \exp\left(\frac{\Delta s_e \Delta T}{k_B T}\right) \exp\left(-\frac{B'}{T\Delta T^2}\right) \Delta T/\beta\right) \quad (6)$$

Here β is the temperature scan rate (e.g. 2 K·min^{-1}) applied during the cooling ramps. Eq (6) is obtained by simply combining Eqs (2) and (3) and replacing t with $\Delta T/\beta$. Using this method, May et al. [11] obtained values for A and B' of 0.013 s^{-1} and 2.1×10^4 K^3, respectively. Subsequently, using larger, 2nd generation HPS-ALTA cells, Lim et al. [10] obtained comparable values of 0.023 s^{-1} and 3.4×10^4 K^3 for methane hydrate *via* this method. However, this approach was found to underpredict $J(\Delta T)$ relative to those measured directly from fixed temperature induction time experiments [15]. This occurs because the derivation of Eq (6) effectively assumes that upon formation the system has been subjected to the same subcooling over the entirety of the preceding portion of the temperature ramp. In reality, the system has experienced a subcooling that constantly increased over the ramp duration. Since the model effectively overestimates the time spent at the subcooling where formation occurred, the fitting process yields an incorrect, lower value of J required to force agreement between the model and the experimental data.

Model Description

This problem can be avoided through the use of the hazard rate function, which accounts for the system's history through the factor $(1 - F(t))$ representing the probability formation has not occurred up to time t, in the denominator. The hazard function's definition reflects the

conditional probability that hydrate formation will occur in the next time (or subcooling) interval, as quantified by the probability density distribution, *given* that it has not yet occurred, as quantified by the complement of the cumulative probability distribution. For a ramped-temperature experiment in which J is not constant, the value of the hazard function at the subcooling where a formation event occurs is given by

$$h(\Delta T) = \frac{f(\Delta T)}{1 - F(\Delta T)} \tag{7}$$

When analysing a distribution of measured formation events, the value of $h(\Delta T)$ (in K^{-1}) is defined for all subcooling bins in which formation occurred. Subcooling-dependent nucleation rates (in s^{-1}) can then be estimated from this hazard rate function by multiplying $h(\Delta T)$ by the cooling rate, β [23].

$$J(\Delta T) = h(\Delta T)\beta \tag{8}$$

This approach was employed by Al-Mukadam et al. [33], who used an integrated (cumulative) hazard function to estimate nucleation rates of lithium disilicate from constant cooling measurements. The equilibrium melting temperature for this system is 1033 K and, at subcoolings of over 684 K, multiple nucleation processes could be discerned from their cooling ramp data. The analysis presented in Equations (7) and (8) is mathematically similar to that of Maeda for gas hydrate nucleation [34] if the survival function, $S(t) = 1 - F(t)$ is substituted.

$$h(\Delta T) = \frac{-S'(\Delta T)}{S(\Delta T)} = -\frac{d}{dt}\ln\left(S(\Delta T)\right) \tag{9}$$

Maeda [34] extracted nucleation rates for hydrates formed from a gas mixture using Equation (9) by evaluating the analytic derivative of a power-law fit to $\ln(S(t))$. While the use of a power-law fit does facilitate an estimate of the trend in J with ΔT, Eqs (7) and (8) can be used directly with the raw experimental data without the need to assume the data are described by a particular analytic function. One disadvantage of fitting an analytic function and then evaluating the

derivative is the potential to artificially smooth the resulting "nucleation [rate] curve" [34]. Additionally, the assumed analytic form of $\ln(S(t))$ imposes a symmetry in $f(t)$ about the mean subcooling. Such symmetry is unlikely for constant cooling experiments where formation events are measured over a wide ΔT range if the accessible number of nucleation sites in the system grows with ΔT. In this case, the survival probability would decrease rapidly at higher subcoolings, yielding a non-symmetric $f(t)$. This effect is especially relevant for experiments conducted at higher cooling rates which tend to sample formation events at higher subcoolings [35].

Here, we use the hazard rate function directly to extract stationary nucleation rates for methane hydrate measured over a range of subcoolings by constant cooling experiments in a second generation HPS-ALTA system [11, 12, 15, 19, 20, 27, 36]. Importantly, the method allows the determination of nucleation rates at subcoolings which are inaccessible with practical induction time experiments. We demonstrate how such experiments when used with this improved analysis method can explore how different classes of heterogeneous nucleation sites contribute to the observed nucleation rate at different subcoolings. Such information provides insight into the mechanisms available for controlling or manipulating gas hydrate nucleation rates.

Experimental Method

Second generation HPS-ALTA cells were used here to measure subcooling distributions of methane hydrate formation at cooling rates of (1 and 3) $K \cdot min^{-1}$. As nucleation rates depend on system size and shear, we followed the method detailed by Lim et al. [10] to hold these parameters constant and facilitate appropriate comparisons to previous work [15, 36, 37]. For a quantitative discussion of the impact of shear and system size on experimental measurements of hydrate nucleation rate, the interested reader is referred to May et al. [11], Metaxas et al. [20] and Jeong et al. [21].

A total of (408 and 456) independent methane hydrate formation events were measured at these respective cooling rates. The subcooling corresponding to each distinct hydrate formation event was used subsequently to construct a histogram from which a probability distribution could be approximated. Briefly, the apparatus consists of numerous stainless-steel, hydrate-forming, stirred reactors (Figure 1). Two cells, each with an internal volume of 10.9 mL, were used in this work. A 100 Ω platinum resistance temperature detector (RTD) inserted into each cell body was used to measure the cell temperature, with the cell pressures measured using inline pressure transducers. Mixing of the fluids within each cell (at 700 RPM) was achieved using a cross-shaped PTFE stir bar driven by magnetic stirrer drive units located under each cell. Six Peltier elements located on the exterior side faces of the hexagonal cell body provided temperature control and enabled rapid heating and cooling of the low-thermal-mass cells.

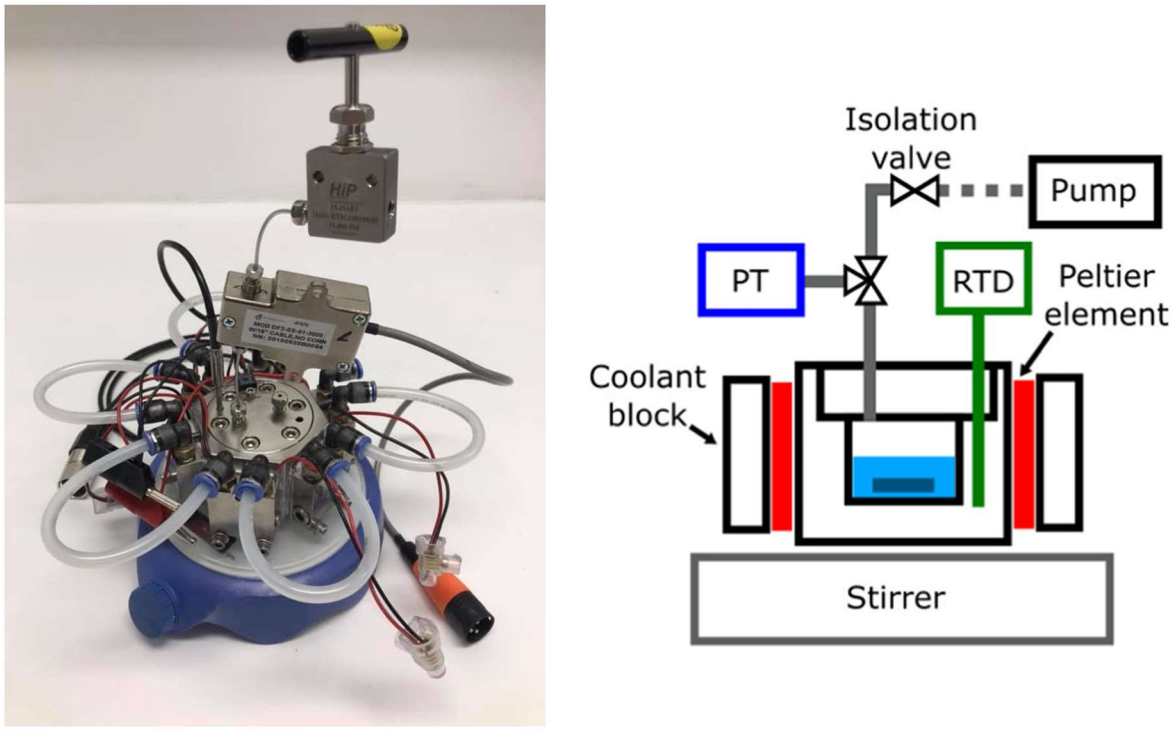

Figure 1: A second generation HPS-ALTA cell mounted on a magnetic stirrer and a simplified schematic.

Approximately 5 mL of degassed, deionised water was loaded into each cell, which was subsequently purged three times with methane (99.995%) at 5 MPa. Following purging, each

cell was pressurised to initialisation conditions of (13 MPa, 20 °C), with the aqueous phase being continuously mixed to ensure uniform dissolution of methane. The cell was then heated to 40 °C and cooled isochorically into the hydrate equilibrium region at a rate of (1 or 3) $K \cdot min^{-1}$. The onset of hydrate formation was detected was detected from the resultant pressure reduction *via* the method described in ref. [10]. The subcooling at formation was calculated using Eq (1) using the formation temperature, T, and the hydrate equilibrium temperature at the formation pressure, T_{eq}, calculated using the CPA-InfoChem equation of state implemented in Multiflash 7.0 [38]. The subcoolings measured for each hydrate formation event in a given cell were combined and used to construct a histogram approximating the probability density distribution for hydrate formation as a function of subcooling. The choice of an appropriate bin width for use in constructing the histogram is non-trivial; we selected 0.3 K based on the Freedman – Diaconis rule [39] where the bin width, δT, is given by

$$\delta T = 2\frac{IQR}{n^{1/3}} \tag{10}$$

Here, IQR is the interquartile range (middle 50% of the distribution), and n is the number of formation events. This bin width provided a reasonable balance between resolution and noise. The histogram was then numerically integrated using the trapezoidal rule to generate the cumulative formation probability distribution for hydrate formation as a function of subcooling.

Results

The resulting probability density and cumulative formation probability functions calculated from the measured formation data are displayed in Figure 2, with the summary statistics of these distributions displayed in Table 1. Increasing the ramp rate enables formation kinetics to be probed at higher subcoolings as the system has spent less time in the hydrate stability region

along the cooling path prior to formation (the mean subcooling observed increased from 6.6 K at 1 K·min^{-1} to 7.3 K at 3 K·min^{-1}).

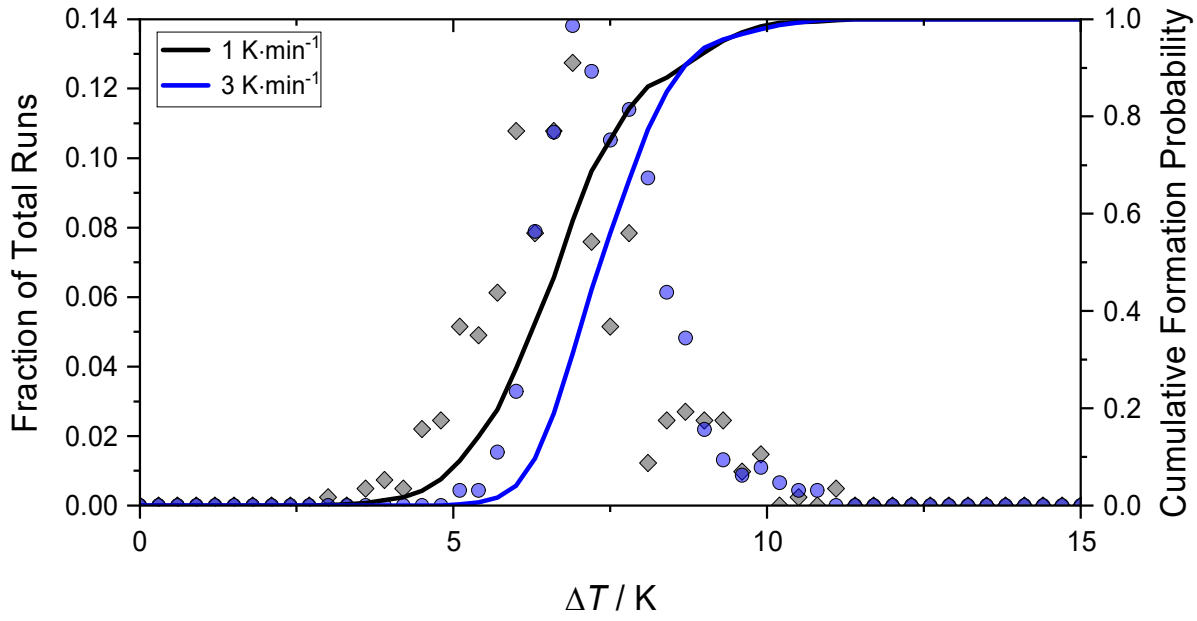

Figure 2: The probability density function (circles) and cumulative distribution function (lines) constructed from binned formation data measured at the experimental cooling rates of (1 and 3) K·min^{-1}. For each ramp rate, the fraction of total runs equals the number of formation events in that subcooling bin divided by the total number of measured formation events. Each subcooling bin contains between 1 and 52 formation events.

Table 1: Summary statistics of the measured formation probability distributions at cooling rates of (1 and 3) K·min^{-1}.

Cooling Rate, β / K min^{-1}	Number of formation events, N	Mean formation temperature, T_f / K	Mean formation pressure, p_f/ MPa	Mean formation subcooling, $\overline{\Delta T}$ / K	Standard deviation in formation subcoolings, σ / K
1	408	281.3	12.11	6.60	1.3
3	456	280.6	11.94	7.28	0.96

The subcooling-dependent nucleation rates were subsequently estimated from the values of the probability density and cumulative probability functions at each bin in which a formation event occurred *via* the hazard rate function (Equations (7) and (8)). The subcooling dependent values of J extracted from experiments at both ramp rates are displayed in Figure 3 alongside those measured for methane hydrate from induction time experiments at fixed subcooling carried out

by Lim et al. [15]. In general, the ramped datasets exhibit good consistency with the isothermal experiments across the range of subcoolings measured, with the scatter of J in the former comparable to that seen for repeat induction time measurements at a constant subcooling [15] Figure 3 also shows a fit of Eq (2) to the data of Lim et al., which has been extrapolated to cover the range of ΔT measured in this work assuming constant values of the best-fit parameters A and B'. The nucleation rate data obtained from cooling ramp experiments using the hazard function analysis method show that this assumption is invalid.

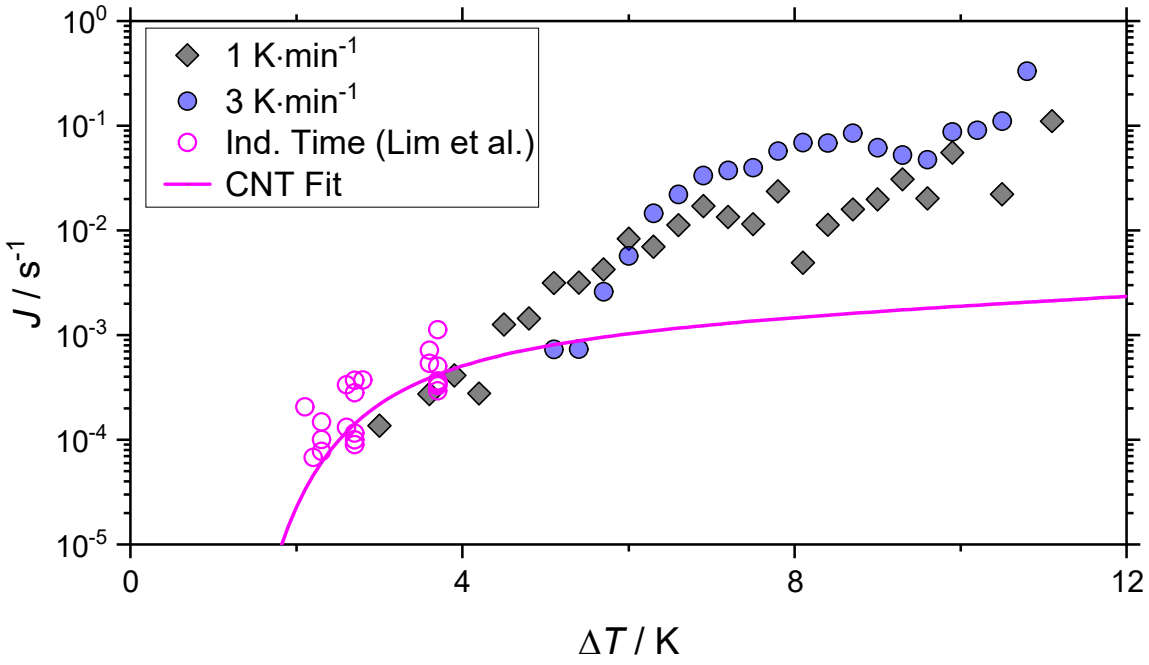

Figure 3: Nucleation rates, J, for methane hydrate extracted from ramped-temperature measurements (via the CDF and PDF displayed in Figure 2) alongside those obtained from constant temperature induction time measurements by Lim et al. [15]. The solid line represents a fit of Equation (2) from Classical Nucleation Theory (CNT) to the data of Lim et al. with $A = 0.001$ s^{-1} and $B' = 4500$ K^3. Below $\Delta T \approx 5$ K, the nucleation rates measured in this work are comparable with those of Lim et al. At higher ΔT, the observed nucleation rate grows more rapidly than predicted by an extrapolation of the fit to data measured at low subcoolings under the assumption that A and B′ remain constant.

The nucleation rates extracted from the constant cooling measurements *via* the hazard function analysis exhibit good consistency with those extracted from isothermal induction time experiments of Lim et al., both in terms of the trends and, for the 1 K·min^{-1} tests, the overlap

in the datasets. This offers validation of the hazard rate analysis method and demonstrates that consistent nucleation rates can be extracted from the two experimental methods, with the constant cooling measurements expanding the range of accessible subcoolings. However, for $\Delta T > 5$ K, the nucleation rates measurable in this work are significantly greater (up to 3 orders of magnitude) than those extrapolated by a fit of Eq. (2) to the data of Lim et al. under the assumption that A and B' remain constant over this extended range of subcooling. This discrepancy arises because the assumption of constant A and B' as subcooling grows becomes increasingly inaccurate for the reasons discussed below.

To explore this observation further, we re-arrange Equation (2) into a linearized form [15, 17, 36]

$$\ln J - \frac{\Delta s_e \Delta T}{k_B T} = \ln(A) - \frac{B'}{T \Delta T^2} \tag{11}$$

and set $y = \ln J - \frac{\Delta s_e \Delta T}{k_B T}$ and $x = 10^4 / T \Delta T^2$. A linear data set in this (x, y) plane indicates a set of subcoolings over which nucleation rates are described by constant values of A and B'. For $x > 1.5$ (approximately equivalent to $\Delta T < 5$ K), the data measured in this work have a linear trend consistent with those of Lim et al.'s for which the best-fit values of A and B' are 0.001 s^{-1} and 4500 K^3, respectively. However, these best-fit parameters clearly do not describe the nucleation rates observed at subcoolings corresponding to $x < 1.5$ ($\Delta T > 5$ K). Instead, the data in this region form a second linear trend characterised by different values of the nucleation parameters. Least squares linear regression of both constant cooling datasets using only the points for which $x < 1.5$, leads to values for A and B' of 0.10 s^{-1} and 3.1 $\times 10^4$ K^3, respectively. Kashchiev and Firoozabadi [17] made a similar observation when constructing a linearised plot of Makogon's methane hydrate nucleation data [40]. They observed that the data point measured at the lowest subcooling (highest x) lay on a different linear trend to those measured

at higher subcooling. They attributed the nucleation rate measured at low subcooling as being caused by sites with significantly lower nucleation work (smaller values of B') than those sites responsible for the nucleation rates observed at higher subcoolings.

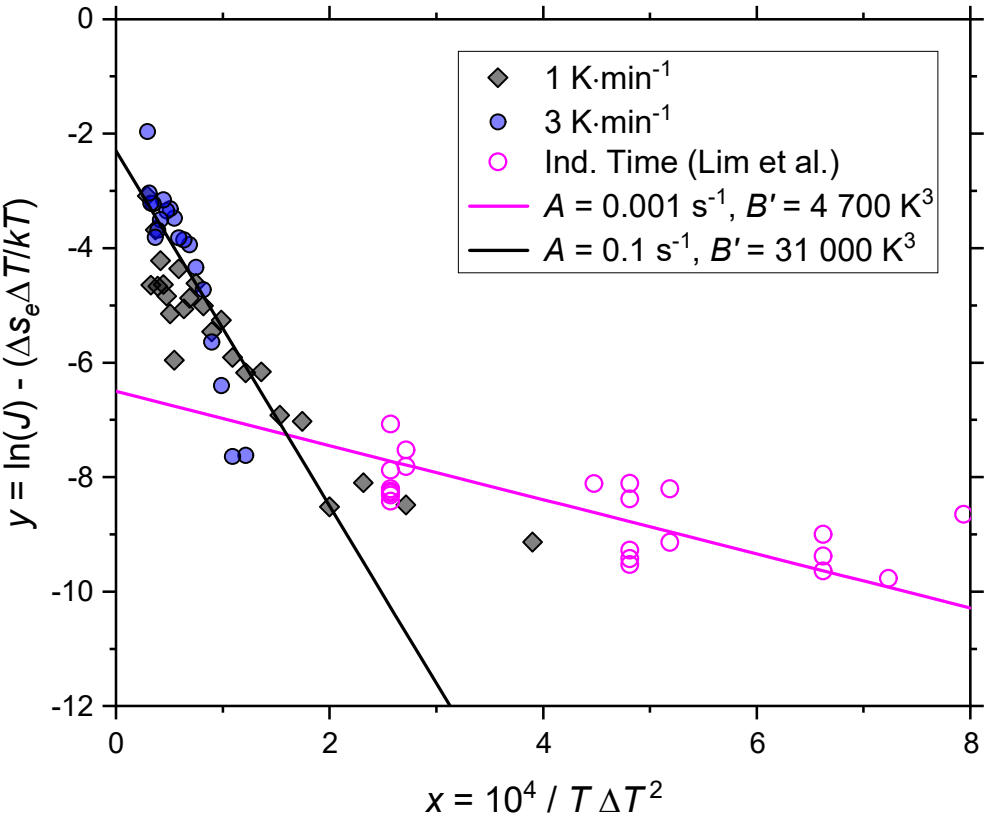

Figure 4: Linearised (x,y) plot of Eqn. (1) for both ramp rates and Lim et al.'s induction time measurements. The thermodynamic nucleation parameter B′ is proportional to the slope, while the kinetic nucleation parameter A is proportional to (the exponent of) the y-intercept of the solid lines respectively. The solid pink line is a fit only to the induction time data of Lim et al., while the solid black line is a fit to the datapoints measured in this work for x < 1.5.

According to CNT, B' is a measure of the nucleation work required at the sites on which nucleation is occurring [17].

$$B' = \frac{4c^3 v_h^2 \sigma_{ef}^3}{27 k_B \Delta s_e^2} \tag{12}$$

Here, c is a shape factor, v_h the volume of a hydrate building unit, and σ_{ef} the energy penalty for introducing the hydrate interface (equivalently, the surface free energy of the hydrate-solution interface). Our analysis suggests that, for $\Delta T > 5$ K, the observed nucleation in the

HPS-ALTA is occurring on a distinct set of nucleation sites characterized by a higher energy barrier than those that responsible for formation at low subcooling (ΔT < 5 K). In isolation, such a seven-fold increase in B' would *decrease* the system's nucleation rate (following Eq (2)). However, in practice this is offset here by the ~100-fold increase in A, which is directly proportional to the number of nucleation sites (N_0) actively contributing to the system's observed nucleation rate.

$$A = zfN_0 \tag{13}$$

Here, z is the Zeldovich factor, and f is the frequency of attachment of hydrate building units to the growing nucleus.

Extracting A and B' from the constant cooling data using the overly simplistic Eq (6) yields respective values of 0.01 s^{-1} and 2.7 $\times 10^4$ K^3 at β = 1 K·min^{-1} and 0.11 s^{-1} and 5.6 $\times 10^4$ K^3 at β = 3 K min^{-1}. Although the thermodynamic nucleation parameters (B') obtained with the two ramp rates are consistent within a factor of 2 with each other and the value determined using the hazard function, the kinetic nucleation parameter A shows a greater dependence on the ramp rate, increasing by an order of magnitude. This is likely an artefact of the model failing to account for the system's history in the hydrate stability region.

Discussion

The method and results presented here for uninhibited systems also help explain formation probability data reported previously for systems with kinetic hydrate inhibitors (KHIs) or different hydrate formers. Lim et al. [15] and Barwood et al. [32] proposed that KHIs extend induction times by eliminating the low-energy heterogenous nucleation sites that determine the J observed at low subcoolings (< 5 K). Their quantitative measurements of CH_4 hydrate nucleation rates in KHI-dosed systems using the HPS-ALTA required significantly higher

subcoolings, at which many more (large A) nucleation sites with high energy (large B') are accessible [15, 36]. Figure 5 shows the nucleation rate data for methane hydrates in the presence of 1 wt% (with reference to the aqueous phase) of polymeric KHIs measured by Lim et al. [15] and Barwood et al. [32], together with the data for uninhibited systems.

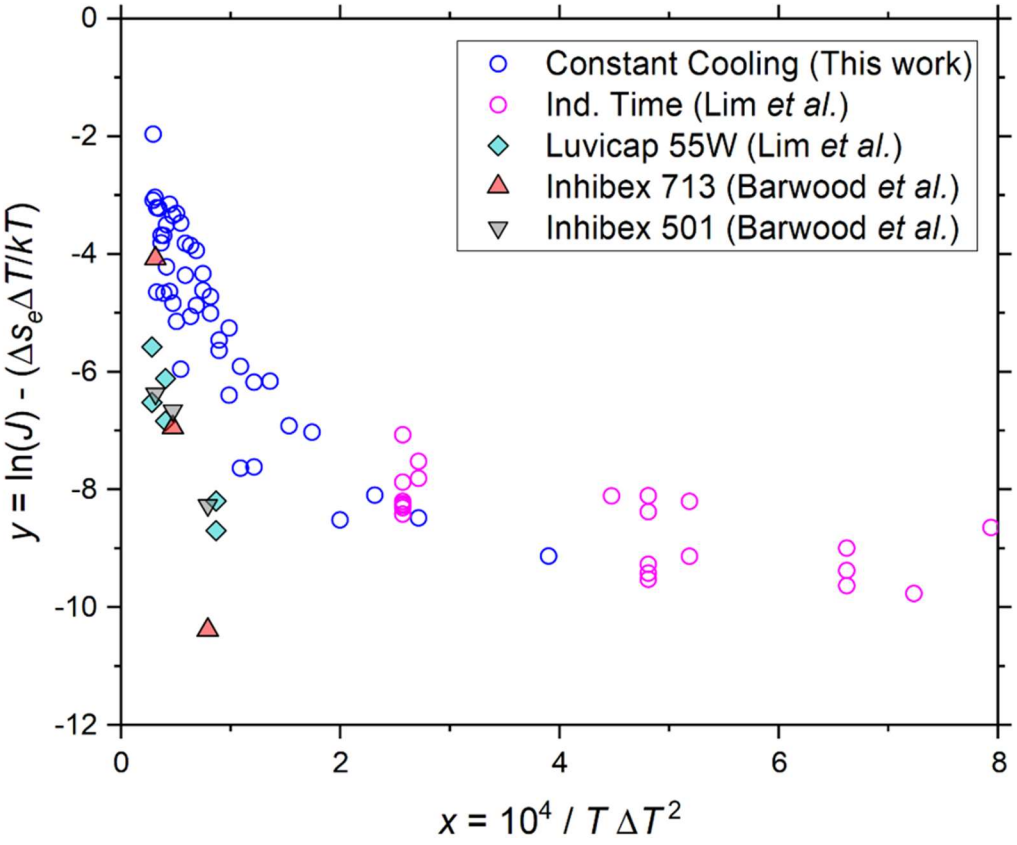

Figure 5: Nucleation rates (in linearised coordinates) at a KHI dosage of 1 wt% (solid symbols) measured at constant temperatures from induction time measurements by Lim et al. [15] and Barwood et al. [36] in the second generation HPS-ALTA, together with the data measured in this work (blue circles) using ramped-temperature experiments, and by Lim et al. for uninhibited methane hydrates (pink circles) at constant temperatures from induction time measurements. The slopes of the data measured for systems with KHI present are similar to those measured at the highest subcoolings accessed by the constant cooling experiments in this work. This suggests that nucleation sites with the same energy barrier contribute to the nucleation rate observed at large subcoolings in both systems.

Conversely, measurements of uninhibited CO_2 hydrates at low subcooling (< 4 K) revealed that fewer sites with lower energy barriers contributed to the observed nucleation rates relative to those measured for CH_4 hydrates in the same HPS-ALTA cells [37]. While the KHI and CO_2

studies explored systems with different values of A and B' by adding inhibitors or changing the hydrate former, this work used an alternate method of determining accurate nucleation rates attributable to more numerous, higher energy nucleation sites accessed by ramped temperature experiments. Interestingly, the value of B' extracted from the high-subcooling data set accessed by rapid cooling rates in this work is in excellent agreement (within a factor of 1.3) of the value obtained from experiments dosed with Inhibex 501 (in [32]) or Luvicap 55W (in [15]). In contrast, the value of A obtained in the presence of a KHI was at least a factor of 7 lower than measured in this work for uninhibited systems. Assuming the KHI does not change z or f in Eq (13) but only reduces the value N_0 corresponding to sites with a given value of B', this suggests that in addition to eliminating the low energy sites, these KHIs can also remove a significant portion of the higher energy sites that become accessible for nucleation when $\Delta T > 5$ K.

Together, these results help establish the conceptual picture of gas hydrate nucleation in the HPS-ALTA experiments displayed in Figure 6. At low subcooling (< 5 K), a small number of low energy sites contribute to the observed nucleation rate. At higher subcoolings (> 5 K), an additional site population (inaccessible at low subcooling due to its high energy barrier) becomes accessible, which consists of many more sites (100-fold). KHIs are able to remove not just the low energy sites, but also eliminate a significant portion of this higher-energy site population and consequently reduce the nucleation rates observed at both high and low subcoolings, relative to those of uninhibited systems.

These results have important implications for characterising gas hydrate formation likelihood in natural gas production systems. They are consistent with, and help interpret, measurements of nucleation rates in the presence of kinetic hydrate inhibitors. Importantly, the observation of that observed nucleation rates in a given system depend on multiple sets of nucleation parameters demonstrates the need to characterise hydrate formation probability over the full subcooling range that is expected to be encountered in an industrial system. The likelihood of

hydrate formation may be significantly under predicted (by up to 3 orders of magnitude) if nucleation rate data obtained at low subcoolings are extrapolated and used in risk-based engineering models.

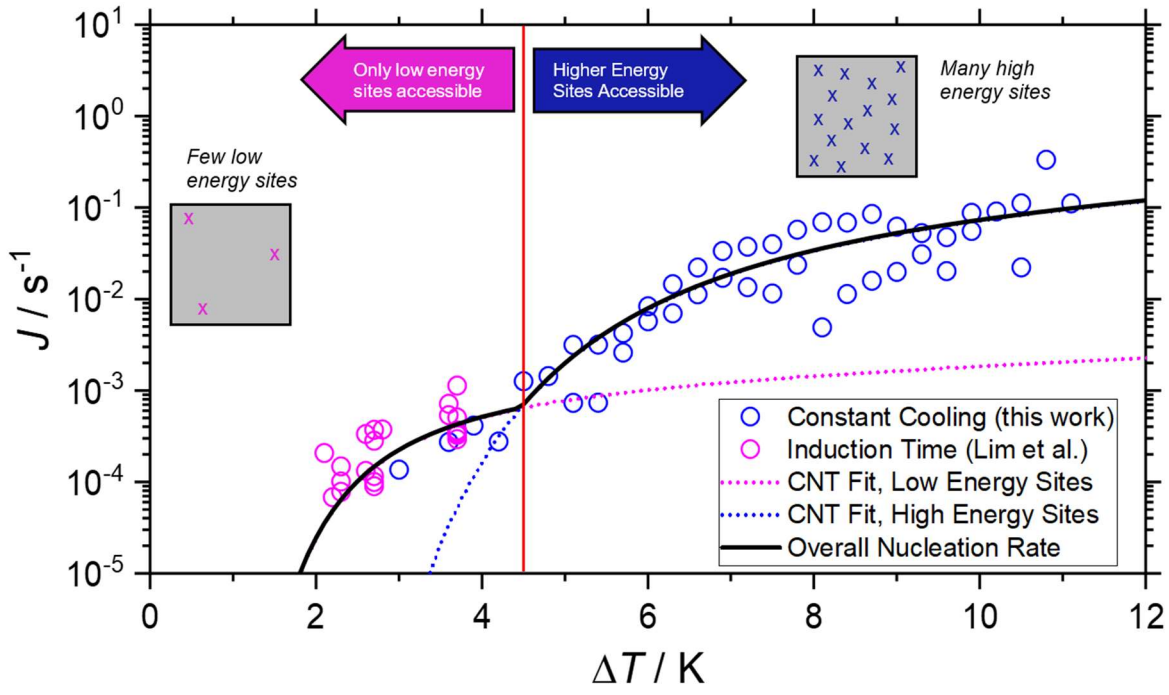

Figure 6: Conceptual picture of methane hydrate nucleation in the HPS-ALTA. At low subcooling, a small number of low energy sites define the nucleation rate. The nucleation rate from these sites expected at higher subcoolings from a CNT fit is indicated by the dashed pink line. However, at higher subcoolings, the measured nucleation rates are greater than this fit due to the contribution of higher energy sites (of which there are many more). These sites do not contribute at low subcooling (represented by the dashed blue line) as they are inaccessible. Thus, the overall nucleation rate can be represented piecewise as the solid black curve.

Conclusions

We have demonstrated the robust extraction of stationary methane hydrate nucleation rates from constant cooling experiments undertaken in a second-generation high pressure stirred, automated lag time apparatus. At the subcoolings accessible in constant temperature experiments, the nucleation rates calculated from this method are in excellent agreement with those extracted by Lim et al. from fixed temperature induction time measurements in the same apparatus [15]. However, the kinetic and thermodynamic nucleation parameters obtained by

Lim et al. from the isothermal data measured in this subcooling range cannot accurately predict the nucleation rates observed at the higher subcoolings made accessible by the ramped temperature experiments used in this work. Analysis of the subcooling dependent nucleation rates data using CNT reveals that the observed hydrate formation can be described by two distinct sets of nucleation parameters. Both A and B' are found to increase as subcooling grows, indicating that both the number of accessible nucleation sites and the corresponding energy barriers of those additional accessible sites also increase. The kinetic and thermodynamic nucleation parameters extracted from the data measured at subcoolings larger than 5 K imply, respectively, that the observed nucleation rate is associated with heterogenous nucleation sites 100 times more numerous but with energy barriers 7 times higher than those determining the nucleation rate at lower subcoolings.

Acknowledgements

This work was funded by the Australian Research Council through FT180100572 and LP200201020. M.T.J.B acknowledges the support of the Australian Government through an Australia Government Research Training Program Fees Offset and the University of Western Australia through a Jean Rogerson Postgraduate Scholarship. We thank Paul Stanwix and Kwanghee Jeong for useful discussions.

References

1. Aman, Z.M., *Hydrate Risk Management in Gas Transmission Lines.* Energy & Fuels, 2021. **35**(18): p. 14265-14282.
2. Sloan Jr, E.D. and C.A. Koh, *Clathrate hydrates of natural gases*. 2007: CRC press.
3. Sloan, E.D., *A changing hydrate paradigm—from apprehension to avoidance to risk management.* Fluid Phase Equilibria, 2005. **228**: p. 67-74.
4. Hassanpouryouzband, A., et al., *Gas hydrates in sustainable chemistry.* Chemical society reviews, 2020. **49**(15): p. 5225-5309.
5. Babu, P., et al., *A review of clathrate hydrate based desalination to strengthen energy–water nexus.* ACS Sustainable Chemistry & Engineering, 2018. **6**(7): p. 8093-8107.
6. Dashti, H., L. Zhehao Yew, and X. Lou, *Recent advances in gas hydrate-based CO2 capture.* Journal of Natural Gas Science and Engineering, 2015. **23**: p. 195-207.
7. Liang, H., et al., *Characterizing Mass-Transfer mechanism during gas hydrate formation from water droplets.* Chemical Engineering Journal, 2022. **428**: p. 132626.
8. Ke, W. and M.A. Kelland, *Kinetic hydrate inhibitor studies for gas hydrate systems: a review of experimental equipment and test methods.* Energy & Fuels, 2016. **30**(12): p. 10015-10028.
9. May, E.F., et al., *Quantitative kinetic inhibitor comparisons and memory effect measurements from hydrate formation probability distributions.* Chemical Engineering Science, 2014. **107**: p. 1-12.
10. Lim, V.W.S., et al., *Gas hydrate formation probability and growth rate as a function of kinetic hydrate inhibitor (KHI) concentration.* Chemical Engineering Journal, 2020. **388**: p. 124177.
11. May, E.F., et al., *Gas hydrate formation probability distributions: the effect of shear and comparisons with nucleation theory.* Langmuir, 2018. **34**(10): p. 3186-3196.
12. Metaxas, P.J., et al., *High-Fidelity Evaluation of Hybrid Gas Hydrate Inhibition Strategies.* Energy & Fuels, 2020.
13. Peytavy, J.-L., P. Glénat, and P. Bourg. *Qualification of low dose hydrate inhibitors (LDHIs): field cases studies demonstrate the good reproducibility of the results obtained from flow loops*. in *Proceedings of the 6th International Conference on Gas hydrates, Vancouver, Canada*. 2008.
14. Duchateau, C., et al., *Laboratory Evaluation of Kinetic Hydrate Inhibitors: A Procedure for Enhancing the Repeatability of Test Results.* Energy & Fuels, 2009. **23**(2): p. 962-966.
15. Lim, V.W.S., et al., *The delay of gas hydrate formation by kinetic inhibitors.* Chemical Engineering Journal, 2021. **411**: p. 128478.
16. Kashchiev, D., *Nucleation*. 2000: Elsevier.
17. Kashchiev, D. and A. Firoozabadi, *Nucleation of gas hydrates.* Journal of Crystal Growth, 2002. **243**(3-4): p. 476-489.
18. Ke, W., et al., *Inhibition–promotion: dual effects of polyvinylpyrrolidone (PVP) on structure-II hydrate nucleation.* Energy & Fuels, 2016. **30**(9): p. 7646-7655.
19. Lim, V.W., et al., *The impact of mono-ethylene glycol and kinetic inhibitors on methane hydrate formation.* Chemical Engineering Journal, 2021: p. 131531.
20. Metaxas, P.J., et al., *Gas hydrate formation probability distributions: Induction times, rates of nucleation and growth.* Fuel, 2019. **252**: p. 448-457.
21. Jeong, K., et al., *Hydrate nucleation and growth on water droplets acoustically-levitated in high-pressure natural gas.* Physical Chemistry Chemical Physics, 2019. **21**(39): p. 21685-21688.

22. Jeong, K., et al., *Gas hydrate nucleation in acoustically levitated water droplets.* Chemical Engineering Journal, 2021: p. 133494.
23. Deubener, J. and J.W.P. Schmelzer, *Statistical Approach to Crystal Nucleation in Glass-Forming Liquids.* Entropy, 2021. **23**(2): p. 246.
24. Gehan, E.A., *Estimating survival functions from the life table.* Journal of Chronic Diseases, 1969. **21**(9): p. 629-644.
25. O'Connor, P. and A. Kleyner, *Practical reliability engineering*. 2012: John Wiley & Sons.
26. Sampson, C.C., et al., *Measurements of solidification kinetics for benzene in methane at high pressures and cryogenic temperatures.* Chemical Engineering Journal, 2021. **407**: p. 127086.
27. Asadi, F., et al., *Cyclodextrins as eco-friendly nucleation promoters for methane hydrate.* Chemical Engineering Journal, 2020: p. 127932.
28. Maeda, N., *Nucleation Curve of Carbon Dioxide Hydrate from a Linear Cooling Ramp Method.* The Journal of Physical Chemistry A, 2019. **123**(37): p. 7911-7919.
29. Maeda, N., *Nucleation curves of methane hydrate from constant cooling ramp methods.* Fuel, 2018. **223**: p. 286-293.
30. Ke, W., T.M. Svartaas, and D. Chen, *A review of gas hydrate nucleation theories and growth models.* Journal of Natural Gas Science and Engineering, 2019. **61**: p. 169-196.
31. Ke, W. and T.M. Svartaas. *Effects of stirring and cooling on methane hydrate formation in a high-pressure isochoric cell*. in *Proceedings of the 7th International Conference on Gas Hydrates, Edinburgh, Scotland, United Kingdom*. 2011.
32. Kulkarni, S.A., et al., *Crystal nucleation kinetics from induction times and metastable zone widths.* Crystal growth & design, 2013. **13**(6): p. 2435-2440.
33. Al-Mukadam, R. and J. Deubener, *Heterogeneous crystal nucleation of supercooled lithium disilicate melt in glassy carbon containers.* Journal of Non-Crystalline Solids, 2021. **571**: p. 121068.
34. Maeda, N., *Nucleation curves of model natural gas hydrates on a quasi-free water droplet.* AIChE Journal, 2015. **61**(8): p. 2611-2617.
35. Heneghan, A. and A. Haymet, *Liquid-to-crystal nucleation: A new generation lag-time apparatus.* The Journal of chemical physics, 2002. **117**(11): p. 5319-5327.
36. Barwood, M.T., et al., *High-resolution performance tests of nucleation and growth suppression by two kinetic hydrate inhibitors.* Chemical Engineering Science, 2021. **244**: p. 116776.
37. Lim, V.W.S., et al., *Nucleation rates of carbon dioxide hydrate.* Chemical Engineering Journal, 2022. **443**: p. 136359.
38. Kontogeorgis, G.M., et al., *Ten years with the CPA (Cubic-Plus-Association) equation of state. Part 1. Pure compounds and self-associating systems.* Industrial & engineering chemistry research, 2006. **45**(14): p. 4855-4868.
39. Freedman, D. and P. Diaconis, *On the histogram as a density estimator: L 2 theory.* Zeitschrift für Wahrscheinlichkeitstheorie und verwandte Gebiete, 1981. **57**(4): p. 453-476.
40. Makogon, Y.F., *Hydrates of hydrocarbons.* 1997.